


ORIGINAL ARTICLE

Enhanced glucose metabolism mediated by CD147 is associated with ¹⁸F-FDG PET/CT imaging in lung adenocarcinoma

Yufan Zhang^{1,2,3,4†}, Jianjing Liu^{1,2,3,4†}, Yunchuan Sun^{5†}, Xiaozhou Yu^{1,2,3,4}, Jian Wang^{1,2,3,4}, Dong Dai^{1,2,3,4}, Yanjia Zhu^{1,2,3,4}, Xiuyu Song^{1,2,3,4}, Lei Zhu^{1,2,3,4}, Xiaofeng Li^{1,2,3,4} & Wengui Xu^{1,2,3,4} 

1 Department of Molecular Imaging and Nuclear Medicine, Tianjin Medical University Cancer Institute and Hospital, Tianjin, China

2 Tianjin Medical University Cancer Institute and Hospital, National Clinical Research Center for Cancer, Tianjin, China

3 Key Laboratory of Cancer Prevention and Therapy, Tianjin, China

4 Tianjin's Clinical Research Center for Cancer, Tianjin, China

5 Department of Nuclear Medicine, Hebei Province Cangzhou Hospital of Integrated Traditional and Western Medicine, Cangzhou, China

Keywords

¹⁸F-FDG PET/CT imaging; CD147; glucose metabolism; lung adenocarcinoma.

Correspondence

Lei Zhu, Department of Molecular Imaging and Nuclear Medicine, Tianjin Medical University Cancer Institute and Hospital Huan-Hu-Xi Road, Ti-Yuan-Bei, He Xi District, Tianjin 300060, PR China
Tel: +86 13752097226
Fax: +86 22 2334 0123
Email: leizhu@tmu.edu.cn

Xiaofeng Li, Department of Molecular Imaging and Nuclear Medicine, Tianjin Medical University Cancer Institute and Hospital Huan-Hu-Xi Road, Ti-Yuan-Bei, He Xi District, Tianjin 300060, PR China
Tel: +86 187 2250 6643
Fax: +86 22 2334 0123
Email: 18722506643@163.com

Wengui Xu, Department of Molecular Imaging and Nuclear Medicine, Tianjin Medical University Cancer Institute and Hospital Huan-Hu-Xi Road, Ti-Yuan-Bei, He Xi District, Tianjin 300060, PR China
Tel: +86 186 2222 1310
Fax: +86 22 2334 0123
Email: wenguixu@yeah.net

[†]Yufan Zhang, Jianjing Liu, and Yunchuan Sun contributed equally to this work

Received: 18 December 2019;

Accepted: 19 February 2020.

doi: 10.1111/1759-7714.13383

Thoracic Cancer **11** (2020) 1245–1257

Abstract

Background: Lung adenocarcinoma (LUAD) is one of the most deadly thoracic tumors. Reprogrammed glycolytic metabolism is a hallmark of cancer cells and significantly affects several cellular functions. In the current study, we aimed to investigate cluster of differentiation 147 (CD147)-mediated glucose metabolic regulation in LUAD and its association with ¹⁸F-FDG PET/CT imaging.

Methods: The expression profile and prognostic potential of CD147 in LUAD were analyzed using UALCAN and a Kaplan-Meier plotter. Tissue immunohistochemical analyses and PET metabolic parameters were used to identify the relationship between CD147 expression and reprogrammed glycolysis. The role of CD147 in glucose metabolic reprogramming was assessed by radioactive uptake of ¹⁸F-FDG through γ -radioimmunoassays in vitro and micro-PET/CT imaging in vivo. Western blotting assays were used to determine the expression level of monocarboxylate transporter 1 (MCT1) and MCT4 in established human LUAD cell lines (ie, HCC827 and H1975) with different CD147 expression levels via lentiviral transduction.

Results: CD147 was highly expressed in LUAD. A significant positive correlation existed between CD147 expression and PET metabolic parameters (SUVmax, SUVmean, SUVpeak). CD147 could promote radioactive uptake of ¹⁸F-FDG in vitro and in vivo, suggesting the ability of CD147 to enhance glycolytic metabolism. Furthermore, as an obligate chaperone for MCT1 and MCT4, CD147 positively correlated with MCT1 and MCT4 expression in LUAD tissues and established cell lines with different CD147 expression.

Conclusions: Our study revealed that CD147 is a promising novel target for LUAD treatment and CD147-mediated glucose metabolism demonstrated its contribution to the predictive role of ¹⁸F-FDG PET/CT imaging for targeted therapeutic efficacy.

Introduction

Lung cancer is the leading cause of cancer-related death among men and women globally. It has been estimated that one-quarter of all cancer deaths were due to lung cancer in 2019 in the United States.¹ Non-small cell lung cancer (NSCLC), which includes squamous cell carcinoma, adenocarcinoma and large cell carcinoma, accounts for the vast majority of all new lung cancer cases.² Within NSCLC, adenocarcinoma is one of the most common histological subtypes.³ Despite great improvements in lung adenocarcinoma (LUAD) research and treatment, the prognosis for LUAD patients remains poor.⁴ Thus, a better understanding of the molecular mechanisms driving the tumorigenesis of LUAD is essential and may enable the development and optimization of therapeutic strategies.

Metabolic alteration, a hallmark of tumor cells, significantly affects various cellular functions, including proliferation and survival.⁵ Specific metabolic activities participate directly in cancer cell proliferation to support tumor growth. Enhanced aerobic glycolysis, which is also known as the Warburg effect,⁶ involves the propensity for proliferating cells, including cancer cells, to take up glucose and secrete the carbon as lactate even when oxygen is present. Thus, cancer cells exhibit increased glucose uptake and an enhanced glycolysis rate even in the presence of oxygen.⁷ The widespread application of ¹⁸F-fluoro-2-deoxyglucose positron emission tomography (¹⁸F-FDG PET) imaging in initial and differential tumor diagnoses, clinical staging, and therapeutic effect evaluation utilizes the hallmarks of upregulated glycolysis in tumor cells.^{8,9} Therefore, ¹⁸F-FDG PET data have emphasized the sheer preponderance of elevated glucose trapping in cancer.

Cluster of differentiation 147 (CD147), also known as extracellular matrix metalloproteinase inducer (EMMPRIN) or basigin, is a broadly expressed cell surface glycoprotein that belongs to the immunoglobulin superfamily.¹⁰ As previously reported, CD147 is highly expressed in numerous cancer types and has been demonstrated to significantly contribute to tumor growth, metastasis and angiogenesis through stimulation of the production of hyaluronan, multiple matrix metalloproteinases (MMPs), and vascular endothelial growth factor A (VEGF-A).^{11–13} CD147 has been suggested as an early diagnostic biomarker and a significantly unfavorable prognostic indicator^{14,15}; this feature makes CD147 of interest for further investigation, not only as a biological marker but also as a potential therapeutic endpoint or target.¹⁶ More importantly, CD147, as an essential chaperone, could form complexes with monocarboxylate transporters (MCTs), which suggests a pivotal role of CD147 in the regulation of cell metabolism. Previous studies have shown that the silencing of CD147 dramatically decreases the glycolytic rate and lactate efflux in carcinoma

cell lines, indicating the involvement of CD147 in tumor glycolysis.^{17–21} However, the involvement of CD147 in reprogramming glucose metabolism in LUAD has not been well elucidated.

In the present study, we first explored the key role of CD147 in LUAD through bioinformatics analyses. Second, we retrospectively analyzed the correlation between the immunohistochemical (IHC) expression of CD147 and the following ¹⁸F-FDG PET metabolic parameters in 70 LUAD patients: maximum, mean, and peak standardized uptake values (i.e., SUVmax, SUVmean and SUVpeak, respectively). We then established several stable LUAD cell lines with different levels of CD147 expression and performed a γ -radioimmunoassay experiment to determine the radioactive uptake of ¹⁸F-FDG in vitro. In addition, we evaluated the performance of CD147 in vivo through ¹⁸F-FDG micro-PET/CT imaging of human LUAD xenograft models in nude mice. Lastly, we detected the association between CD147 and MCT1 and MCT4 expression in LUAD tissues and established human LUAD cell lines. Enhanced glucose metabolism mediated by CD147 upregulation was demonstrated to significantly contribute to ¹⁸F-FDG PET/CT imaging in LUAD.

Methods

Patients and tissue samples

A total of 70 LUAD patients who underwent ¹⁸F-FDG-PET/CT scans before operation and/or other therapeutic interventions in our center from January 2018 to January 2019 were included. The clinicopathological characteristics of the patients are summarized in Table 1. Written informed consent forms were obtained from each patient. All specimens were surgically resected from hospitalized patients with complete clinical information and pathologically confirmed as LUAD. Corresponding formalin-fixed paraffin-embedded tissue samples were retrieved from the

Table 1 Clinicopathological characteristics of the patients enrolled in this study (*n* = 70)

Items	Characteristics	<i>N</i>	%
Gender	Male	36	51.4
	Female	34	48.6
Age, mean (range)	< 60	32	45.7
	≥ 60	38	54.3
Smoking	Yes	41	58.6
	No	29	41.4
Lymphatic metastasis	Yes	8	11.4
	No	62	88.6
Clinical staging	I or II	54	77.1
	III or IV	16	22.9

archives of the Department of Pathology in our affiliate institution. This study was approved by the ethics committee of Tianjin Medical University Cancer Institute and Hospital and was conducted in accordance with the Declaration of Helsinki.

Cell lines and animals

A total of four human LUAD cell lines (i.e., HCC827, H1975, PC9 and A549) were used in this study. The HCC827 cell line and H1975 cell line were purchased from the Cell Bank of the Chinese Academy of Sciences (Shanghai). The A549 cell line and PC9 cell line were kindly provided by the Central Laboratory of Tianjin Medical University Cancer Institute and Hospital. The cells were regularly cultured in Dulbecco's modified eagle medium (DMEM) supplemented with penicillin/streptomycin (1:200) and 10% fetal bovine serum (FBS) at 37°C in a humidified atmosphere containing 5% CO₂ and 95% O₂. Approximately six-week-old immunodeficient female specific pathogen-free (SPF) BALB/c nude mice (Biotechnology Co., Ltd., Beijing) with an average bodyweight of 20 g were used in the present study. The total number of animals used in this study was 30. The mice were housed with ad libitum food and water in groups of five under SPF, controlled ambient conditions. All protocols involving animals were in strict accordance with the recommendations in the Guide for the Care and Use of Experimental Animals of the National Institutes of Health and were approved by the Animal Ethical Review Committee of Tianjin Medical University Cancer Institute and Hospital.

Bioinformatics analysis

UALCAN (<http://ualcan.path.uab.edu/analysis.html>)²² is an online tool to analyze the gene expression profile of different tissues (primary tumor and normal) from The Cancer Genome Atlas (TCGA). Thus, we could verify the expression levels of CD147 and MCT genes in LUAD patients (primary tumor and normal tissues). A *P*-value <0.05 was considered statistically significant. The Kaplan-Meier plotter web server (<http://kmplot.com/analysis/>)²³ was used to analyze the prognostic significance of CD147 and MCT genes in 1926 lung cancer patients and 720 LUAD patients, respectively. The plotter enables users to separate patients into high and low expression groups based on the gene transcription expression level of a given gene and create Kaplan-Meier plots. In addition, the hazard ratio and 95% confidence interval and the log-rank *P*-value were calculated and are shown in the tables, and the number-at-risk is displayed below the curves.

18F-FDG PET/CT imaging

All ¹⁸F-FDG PET/CT scans were conducted using a GE Discovery Elite PET/CT scanner (GE Medical Systems, Waukesha, WI, USA). Patients were required to fast for six hours prior to the scan. Before intravenous injection of ¹⁸F-FDG, the plasma glucose concentrations of patients were examined and maintained under a level of 6.8 mmol/L. The administered activity of the radiotracer was 4.1–4.8 MBq (0.11–0.13 mCi) per kilogram bodyweight. Images were acquired from head to mid-thigh approximately one hour after ¹⁸F-FDG injection. CT scans were performed with the following parameters: current, 120–170 mA; voltage, 120 kV; slice thickness, 5 or 3.75 mm; and reconstruction interval, 5 or 3.75 mm. Afterward, CT-based attenuation-corrected PET images were acquired in three-dimensional mode with two minutes per bed position and were reconstructed using an iterative algorithm with a 192 × 192 matrix. In addition, a noncontrast CT scan targeted to the lung lesion with a slice thickness of 1.25 mm was also obtained for each patient. PET metabolic parameters were automatically generated by PETVCAR, a semiquantitative software embedded in GE workstation (estimated threshold for discrimination of tumors was chosen as equaling to or more than 42% of SUV_{max}). SUVs were calculated according to the following formula: SUV = radioactivity concentration/ (injected activity/ bodyweight).

Immunohistochemistry

IHC analyses were performed on formalin-fixed, paraffin-embedded sections of the surgical specimen. The paraffin blocks were cut to a 4 μm thickness. Briefly, tissue sections were heated at 55°C –60°C for three hours, dewaxed, and rehydrated with xylene and a series of grades of alcohol. Antigen retrieval was performed in citrate buffer (0.01 M, pH 6.0) for three minutes with microwaves. After inactivation of endogenous peroxidase with 3% hydrogen peroxide for 20 minutes, the sections were blocked with 10% normal goat serum at room temperature for 10 minutes and then incubated overnight at 4°C with a series of primary antibodies (i.e., anti-CD147, anti-MCT1, and anti-MCT4, 1:100, Santa Cruz Biotechnology, Dallas, TX). After incubation with a biotin-conjugated secondary antibody for one hour at room temperature, the sections were continued with 3, 3'-diaminobenzidine for visualization. In addition, all sections were counterstained with hematoxylin, followed by dehydration and mounting. Phosphate-buffered saline (PBS) was used instead of primary antibodies for the negative control. Stained slides were scored blindly by two pathologists and photographed under a bright field

microscope. CD147, MCT1, and MCT4 expression levels were determined by examination of the percentage of positively stained cells and the intensity of the cytoplasm and cell membrane staining. The scored area was the entire specimen. The percentage of immunoreactivity was graded on a scale of 0 to 3 (0 for $\leq 5\%$ positive cells, one for 5% to 25% positive cells, two for 25% to 50% positive cells, and three for $>50\%$ positive cells). The staining intensity was stratified into the following three categories: 0 for no staining or pale yellow staining, one for weak immunoreactivity with brown staining, two for strong immunoreactivity with tan staining. The two scores were multiplied to obtain a composite expression score. The final expression level was classified as negative/weakly positive (\pm) (score = 0), moderately positive (++) (score = 1–3), or strongly positive (+++) (score = 4–6).

Establishment of stable LUAD cell lines with different levels of CD147 expression

Stable LUAD cell lines with different CD147 expression levels were established through lentiviral particle production and lentiviral transduction. Before lentiviral packaging and transduction, a small hairpin RNA (shRNA) targeting the human CD147 mRNA sequence (5'-GTACAAGATCACTGACTCT-3') and the full-length cDNA for human CD147 to induce CD147 expression were cloned into pLL3.7 (EGFP) and pLVX-IRES-ZsGreen lentiviral vectors (Youbao Biotechnology, Changsha, China), respectively. Lentiviral particles were produced by transient cotransfection of HEK 293T cells with pSPAX2 and pMD2.G plus the bidirectional pLVX-IRES-ZsGreen-CD147 or pLL3.7-CD147-shRNA or plus the pLVX-IRES-ZsGreen or pLL3.7 control lentiviral vectors. The particles produced were collected from the culture supernatant 48 hours thereafter. The viral titer was determined by transducing HEK 293T cells with successive dilutions of the supernatant. For lentiviral transduction, HCC827 and H1975 cell lines were transduced with CD147-expressing lentiviral particles or CD147-targeting lentiviral particles at a multiplicity of transduction (MOI) of 10 in the presence of 5 $\mu\text{g/mL}$ PolyBrene (Sigma-Aldrich, Oakville, Canada). Following lentiviral transduction, the cells were continually cultured in complete medium for 10–14 days, and ZsGreen positive-transduced and EGFP positive-transduced HCC827 and H1975 cell lines were then enriched using BD FACSAria (BD Biosciences, San Diego, CA) with a purity of 95%–98% to construct stable LUAD cell lines with different levels of CD147 expression. The level of CD147 expression in these purified transduced cells was tested with a western blotting analysis prior to phenotypic and functional assays.

Western blotting

The total protein was extracted from human LUAD cell lines (HCC827, H1975, PC9, A549), and lentiviral transduced HCC827 and H1975 cells. Briefly, cells were lysed with RIPA buffer (Beijing Solarbio Science & Technology Co., Ltd) supplemented with a protease/phosphatase inhibitor cocktail (Cell Signaling Technology, Beverly, MA), and then equal amounts of protein (30–50 $\mu\text{g/lane}$) were loaded and separated by 10% SDS-PAGE. The proteins separated in the gels were then transferred to polyvinylidene difluoride membranes and blocked with 5% skim milk powder for one hour. Subsequently, the membranes were incubated overnight with primary antibodies at 4°C. Anti-CD147, anti-MCT1 and anti-MCT4 antibodies (Santa Cruz Biotechnology) were used at a dilution of 1:500 and anti-GAPDH (Cell Signaling Technology) was used in the dilution of 1:2000. After washing with TBS containing 0.1% Tween 20, the membranes were incubated with secondary antibody (1:2000; Santa Cruz Biotechnology). The blots were developed with ECL (Millipore, Bedford, MA) plus a Western blotting detection system. The experiment was repeated three times.

Radioactive uptake of 18F-FDG by LUAD cell lines in vitro using γ -radioimmunoassays

To evaluate the correlation between CD147 expression and glucose metabolism in LUAD cell lines, established LUAD cell lines were plated in 12-well plates in triplicate and incubated at 37°C in a 5% CO₂ cell incubator. Then, 24 hours later, the culture medium in every well was replaced with 1 mL 10% FBS-supplemented DMEM without glucose containing 10 μCi ¹⁸F-FDG (synthesized in our laboratory) for different durations (0.5, 1, and 2 hours). Rinsing, digestion, and washing with PBS were performed after incubation to eliminate extracellular activity. Then, single-cell suspensions were prepared in PBS to detect ¹⁸F-FDG uptake by LUAD stable cell lines with different levels of CD147 expression. Radioactivity was measured with a γ -radioimmunoassay counter (Cobra Quantum; Packard), and the results were normalized as the number of radioactive cells per 1×10^5 cells. The experiment was repeated three times.

18F-FDG micro-PET/CT imaging of human LUAD xenograft models with different levels of CD147 expression

Lentiviral transduced HCC827 cells (2×10^6 /mouse) in the logarithmic phase suspended in 100 μL of PBS were subcutaneously injected into the dorsa of the mice. Tumor growth and animal health were monitored twice weekly.

When the xenografts grew to a maximal diameter of 8–10 mm, ^{18}F -FDG micro PET-CT imaging was performed. For each tumor model, the xenografts were imaged after tail vein injections of ^{18}F -FDG at a concentration of 10 $\mu\text{Ci/g}$. Mice were fasted 10 hours before PET scanning. CT was performed followed by PET, and the separate PET and CT images acquired were transferred to a workstation for image fusion. The PET/CT images were then reconstructed with attenuation correction and an ordered-subset expectation maximization iterative algorithm. The images were reviewed using the manufacturer's review station (Xeleris, General Electric Healthcare). The SUVmax of the right versus the left xenograft was calculated as the main outcome measurement.

Statistical analysis

SPSS version 24.0 was used for statistical analyses in this study. Categorical data were expressed as percentages, and numerical data are presented as the mean \pm standard error of the mean. The associations between CD147/MCT1/MCT4 and clinicopathological factors were investigated by Chi-square test. PET metabolic parameters among multiple groups were compared with Kruskal-Wallis test. Correlations between CD147/MCT1/MCT4 expression and PET metabolic parameters were tested by Spearman's rank correlation analysis. Student's unpaired *t*-test and one-way ANOVA were performed to determine the significance of the difference between group means using GraphPad Prism software. When there was a significant difference in one-way ANOVA test, a post-test (Student-Newman-Keuls test, SNK) was performed. A *P*-value of 0.05 was considered to indicate a statistically significant difference.

Results

CD147 overexpression in LUAD contributes to poor overall survival of LUAD patients

TCGA data of LUAD patients are used via the UALCAN data portal. As shown in Fig 1a, TCGA data analysis showed that the mRNA levels of the CD147 gene were highly expressed in tumor tissues of multiple cancer types, including LUAD (Fig 1b). In addition, CD147 expression was positively correlated with disease progression (Fig 1c). Furthermore, the Kaplan-Meier plotter database was used to evaluate the prognostic value of CD147 based on Affymetrix microarrays. Notably, a worse prognosis in lung cancer (Fig 1d) and LUAD (Fig 1e) was shown to correlate with higher CD147 expression.

Association between CD147 expression and PET metabolic parameters in LUAD

A total of 70 cases of LUAD were included in this retrospective study. Based on the results of IHC analyses for CD147, LUAD patients were divided into three groups: negative/weakly positive [\pm], moderately positive [++], or strongly positive [+++]. There was no significant association between CD147 expression and clinicopathological factors (*P* > 0.05). To access the intensity of glucose metabolism within the tumor, PET metabolic parameters, including SUVmax, SUVmean and SUVpeak, were acquired from PETVCAR software. The differences in PET metabolic parameters among the three groups were statistically significant (Table S1). All three PET metabolic parameters were considerably higher in LUAD patients with strongly positive expression of CD147 than that in LUAD patients with negative/weakly positive/moderately positive expression of CD147 (Fig 2b–d). In addition, the Spearman rank correlation analysis between CD147 expression and PET metabolic parameters in LUAD showed that PET metabolic parameters were positively correlated with CD147 status (Table 2). Representative IHC images of CD147 and corresponding PET/CT scans are shown in Figure 2a.

CD147 promoted 18F-FDG uptake in vitro and in vivo

Based on the diverse expression of CD147 in LUAD cells (Fig 3a), we selected the HCC827 and H1975 cell lines for further analysis. The HCC827 cell line had the highest CD147 expression level among the four cell lines (Fig 3b). We successfully generated stable LUAD cell lines with varying levels of CD147 expression (Fig 3c,d). The stable LUAD HCC827 and H1975 cell lines with different levels of CD147 expression were incubated with ^{18}F -FDG in vitro to determine the ^{18}F -FDG uptake values using a γ -radioimmunoassay counter. ^{18}F -FDG uptake was markedly higher in the HCC827-CD147 cell line with CD147 overexpression than in the HCC827 control (*P* < 0.001) and HCC827 CD147 shRNA cell lines (*P* < 0.001) with decreased CD147 expression (Fig 4a). Similarly, CD147 also positively correlated with ^{18}F -FDG uptake in the stable H1975 cell lines with different levels of CD147 (Fig 4b).

To correlate the in vitro results of CD147 silencing and overexpression with an in vivo system, we established human LUAD xenograft models with different CD147 expression levels in nude mice. The main component of H1975 xenografts was cystic, which resulted in the inability to perform a quantitative analysis. Therefore, we selected HCC827 as the tumor-forming cells. Consistent with our cell culture analysis, CD147 overexpression led to significant accumulation of ^{18}F -FDG uptake in the HCC827-CD147

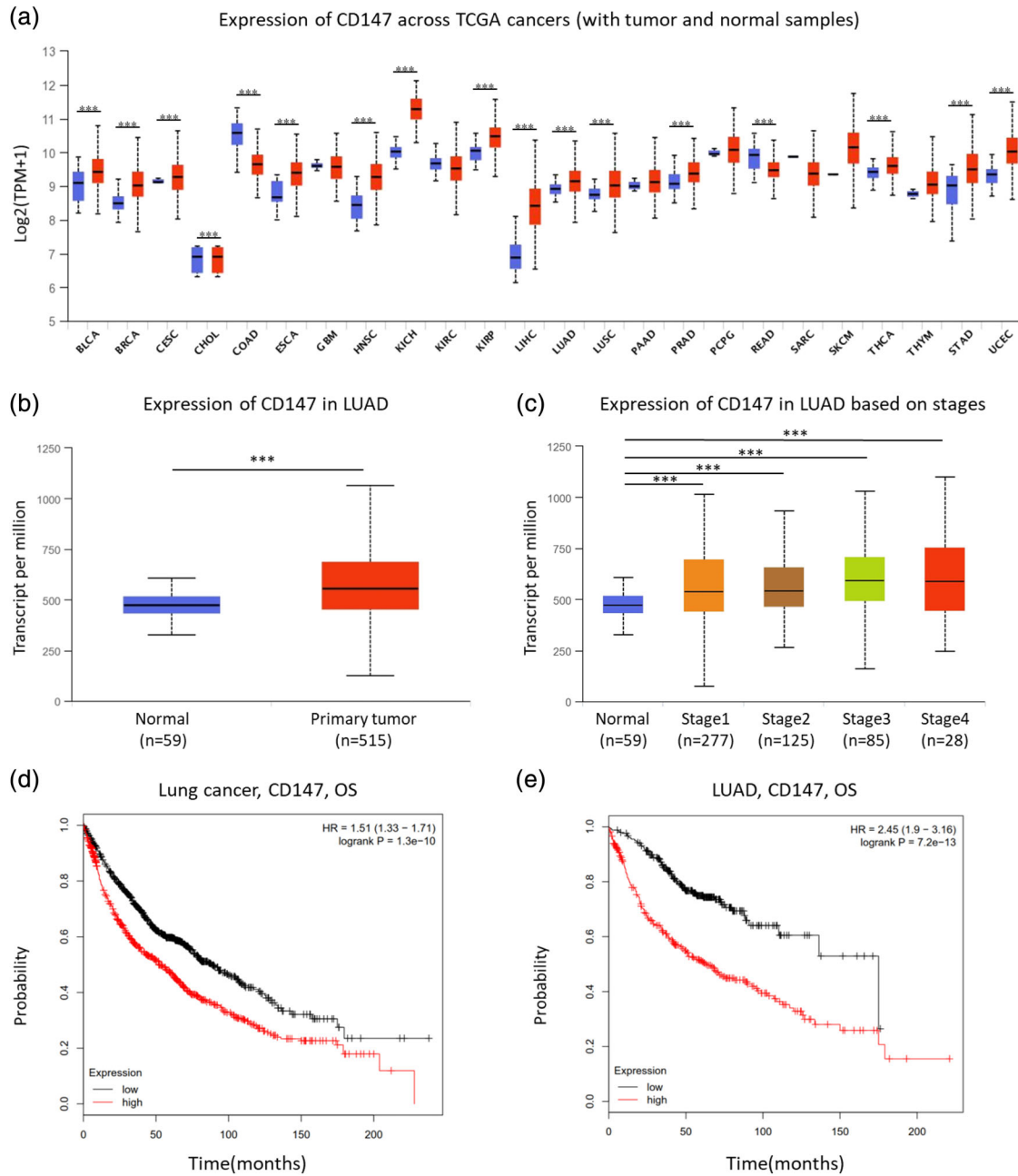


Figure 1 CD147 was overexpressed in lung adenocarcinoma (LUAD), and its expression level was correlated with poor survival (a) CD147 mRNAs level in different tumors and normal tissues of multiple cancer types from TCGA database. (b) A box plot was constructed to represent the differential expression of CD147 mRNAs level between primary tumor tissues ($n = 515$) and normal tissues ($n = 59$) from LUAD patients. (c) CD147 mRNAs level was evaluated in 515 cases LUAD tissues with different disease condition (d) The relationship between CD147 expression and overall survival (OS) in lung cancer ($n = 1926$), described by Kaplan–Meier plotter. Expression —low, —high. (e) Kaplan–Meier survival curves comparing the high and low expression of CD147 in LUAD ($n = 720$) which indicated that OS was significantly higher in the CD147 low expression group than in the high expression group ($***P < 0.001$). Expression —low, —high.

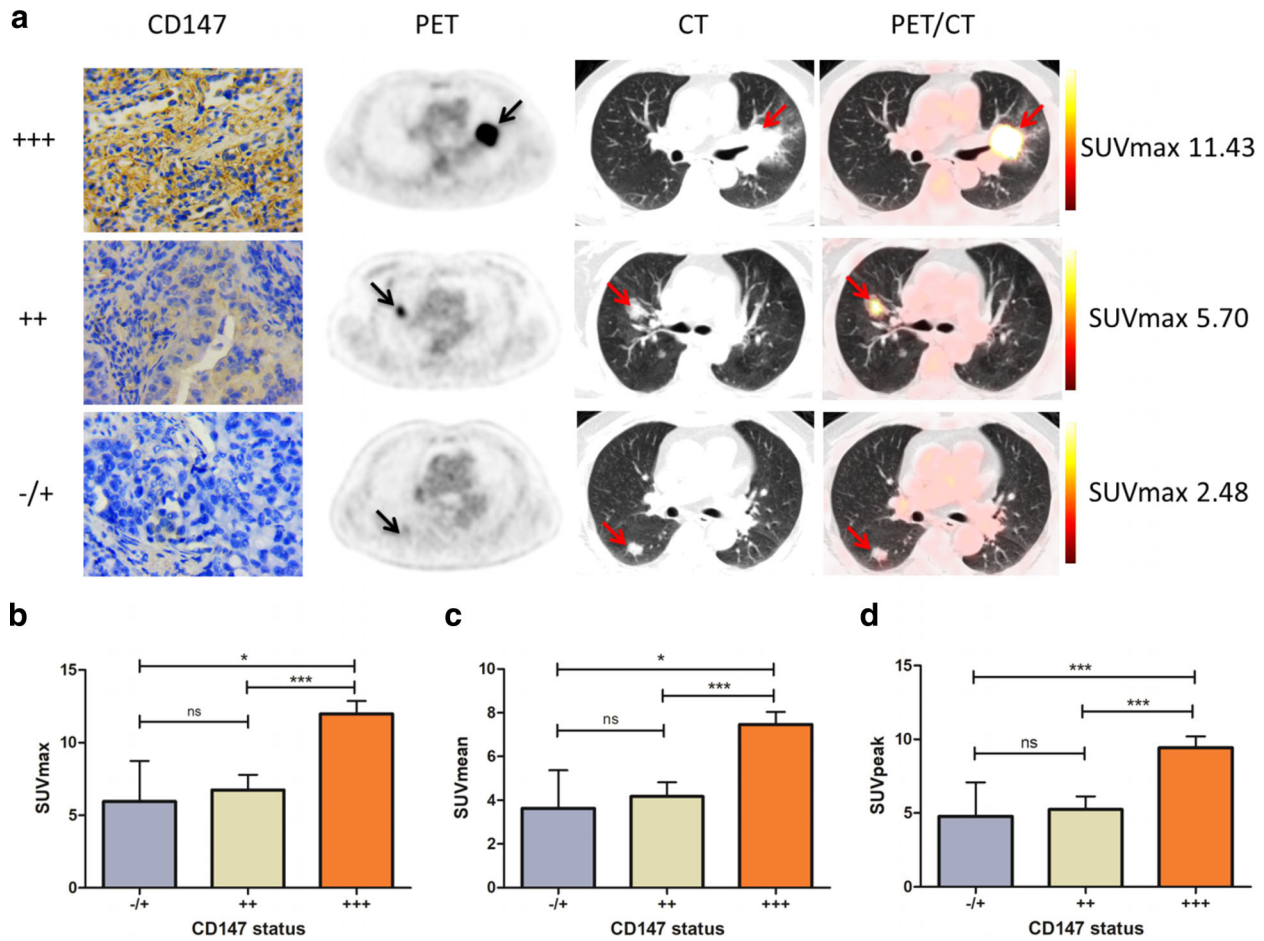


Figure 2 (a) Representative IHC images of CD147 and corresponding 18F-FDG PET/CT scans. Status of CD147 on LUAD tissues was detected by IHC staining. An IHC profile was shown from three representative LUAD patients with weakly positive/negative (±, ×400, lower), positive (++, ×400, middle) and strongly positive (+++, ×400, upper) expression of CD147. Each of the corresponding 18F-FDG-PET/CT images revealed a solitary pulmonary lesion that was suspected to be malignant. SUVmax was 2.48 (lower), 5.70, (middle), 11.43 (upper), respectively. (b, c, d) Histograms were conducted to represent the difference in SUVmax, SUVmean and SUVpeak between different CD147 expression groups. (**P* < 0.05, ****P* < 0.001).

Table 2 Correlation between CD147 status and PET metabolic parameters

PET parameters	CD147 status			R	P-value
	-/+	++	+++		
SUVmax	5.95 ± 2.79	6.74 ± 1.03	11.98 ± 0.89	0.530	<0.001
SUVmean	3.63 ± 1.74	4.17 ± 0.65	7.46 ± 0.58	0.532	<0.001
SUVpeak	4.78 ± 2.30	5.24 ± 0.89	9.43 ± 0.77	0.521	<0.001

xenografts. HCC827CD147 shRNA xenografts demonstrated remarkably lower ¹⁸F-FDG uptake than HCC827-control xenografts (Fig 4c). The SUVmax was used to semi-quantitatively analyze the radioactive uptake of ¹⁸F-FDG by different xenografts. The SUVmax in the HCC827-CD147 xenografts was the highest among all the types of HCC827 xenografts with different CD147 expression levels (Fig 4d).

The accumulation of ¹⁸F-FDG in the HCC827 xenografts was positively correlated with the CD147 expression level. In conclusion, CD147 significantly augmented glucose metabolism in tumor cells in vitro and in vivo. ¹⁸F-FDG PET imaging of nude mice bearing human LUAD xenografts with different levels of CD147 could predict the performance of CD147-mediated glucose metabolism.

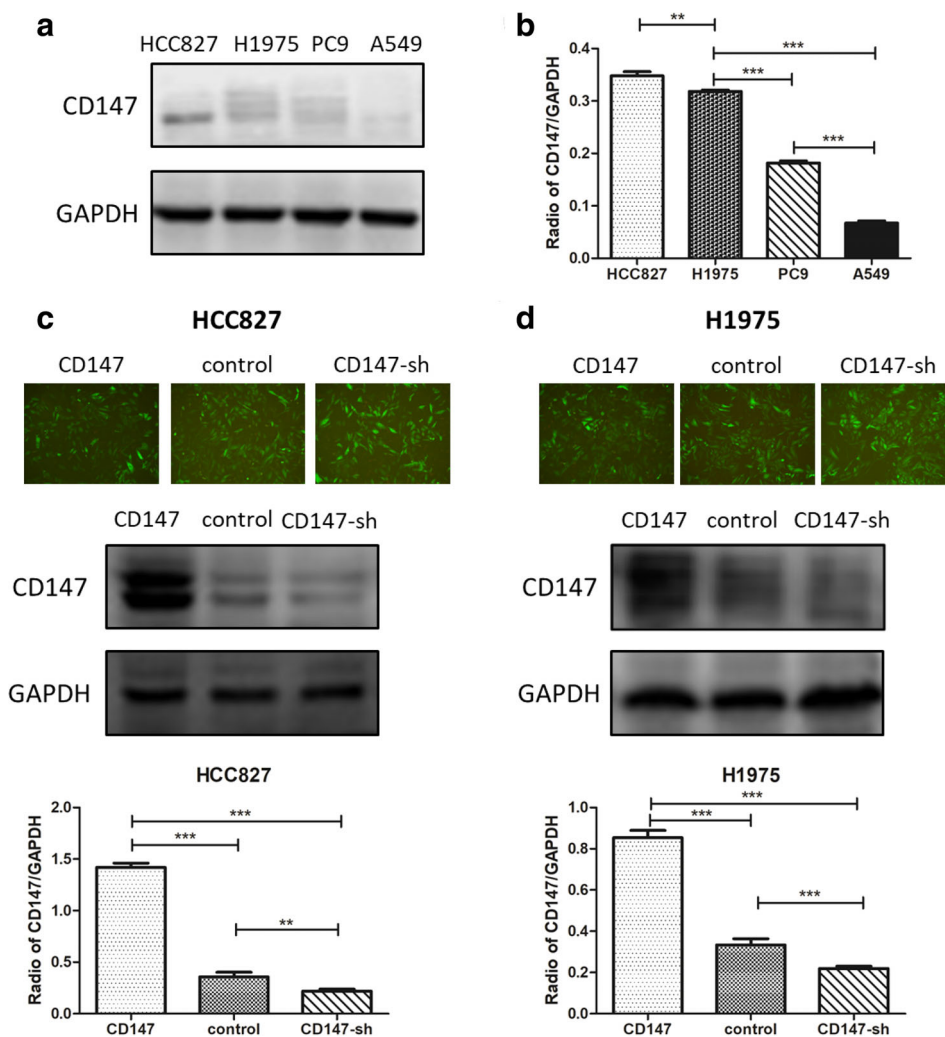


Figure 3 Different levels of CD147 expression in LUAD cell lines and the establishment of stable HCC827 and H1975 cell lines with different CD147 expression levels (a) CD147 expression level was detected by western blotting in four LUAD cell lines. (b) The CD147/GAPDH ratio simply represents the different endogenous level of CD147 in four LUAD cell lines. Statistics showed that HCC827 and H1975 cell line exhibited the highest CD147 expression. (c) Establishment of stable HCC827 cell lines (with GFP) with different levels of CD147 expression through the lentiviral transduction of CD147-expressing lentiviral particles (CD147) and CD147-targeting lentiviral particles (CD147-sh). Verification of CD147 expression was determined by western blotting. (d) Construction of stable H1975 cell lines (with GFP) with different levels of CD147 expression. Different CD147 expression levels were verified by western blotting. GFP, Green fluorescent protein (***P* < 0.01, ****P* < 0.001).

CD147-mediated glucose metabolic regulation of LUAD cell lines relies on MCT1 and MCT4

To determine the specific mechanism of CD147-mediated metabolic regulation in LUAD, we tested the contribution of MCT1 and MCT4 to the phenotype identified above. IHC staining was used to confirm the association between MCT1 and MCT4 expression and CD147 expression in clinical specimens. Representative IHC images of CD147 and MCT1/4 are shown in Figure 5a. As shown in Table 3, CD147 expression positively correlated with MCT1 and MCT4 expression. In addition, there were significant differences in PET metabolic parameters between MCT1 and MCT4 different expression groups (Table S2), and a significantly positive correlation existed in MCT1 and MCT4 expression and PET metabolic parameters (Tables S3, 4). We next detected the expression of MCT1 and MCT4 in lentiviral transduced cells using western blotting assays. Further western blotting analyses indicated that MCT1 and MCT4 expression was considerably

upregulated in HCC827-CD147 and H1975-CD147 cell lines. In contrast, CD147 knockdown significantly decreased the expression of MCTs (Fig 5b,c). Combining all the above results, we demonstrated that CD147-mediated metabolic regulation of LUAD progression relies on MCT1 and MCT4.

Discussion

Lung cancer is a heterogeneous and aggressive disease with an overall five-year survival rate of 15%. Approximately 70% of lung cancer patients are diagnosed with adenocarcinoma, which is the most common histological subtype.²⁴ PET/CT, as a morphological and functional radiographic imaging modality, is widely used for clinical management of lung cancer.²⁵ ¹⁸F-FDG, a radiolabeled glucose analog, has been developed as the most commonly used PET probe to image glucose metabolism in tumors, and the uptake of ¹⁸F-FDG can be semiquantified by PET metabolic parameters with reasonable reproducibility. SUVmax, which

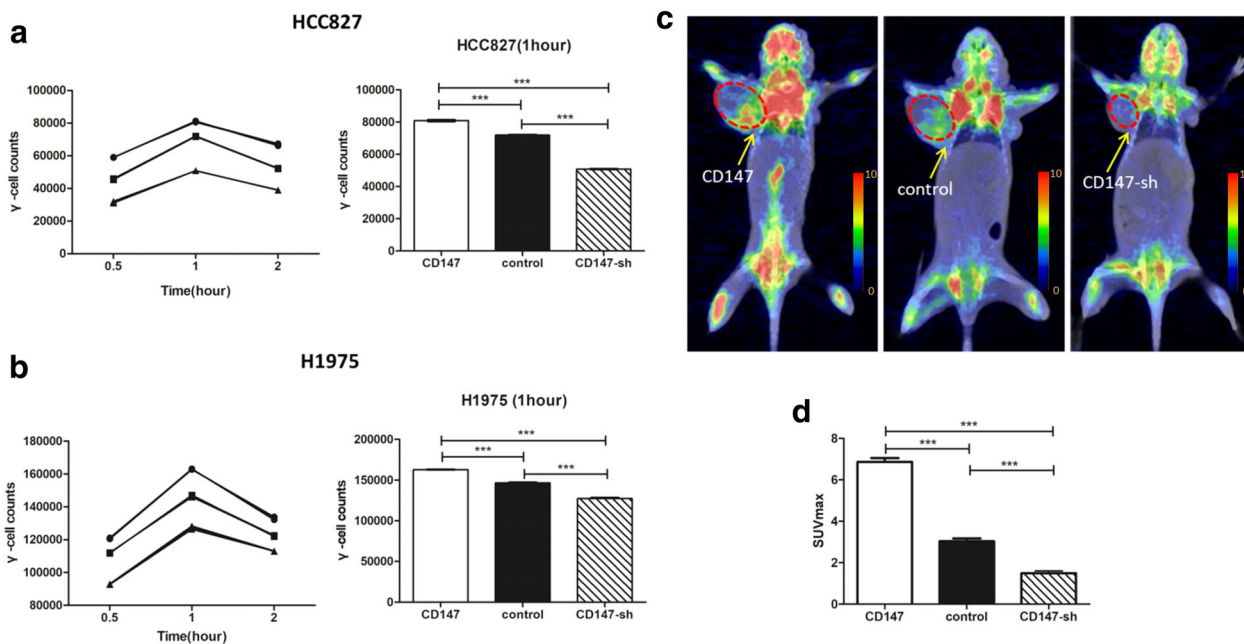


Figure 4 CD147 promoted 18F-FDG uptake in human LUAD cell lines and LUAD xenograft models. **(a, b)** CD147 promoted 18F-FDG uptake by both stable HCC827 and H1975 cell lines with different CD147 expression levels. 18F-FDG was incubated in the culture media of stable HCC827 and H1975 cell lines with different levels of CD147 expression for 0.5, 1, and 2 hours. 18F-FDG uptakes by cell lines in vitro were then measured by a γ -radioimmunoassay. The maximal γ -cell counts were observed with incubation for one hour. As demonstrated, HCC827-CD147 and H1975-CD147 cell lines with CD147 overexpression were found to be able to take up more 18F-FDG compared to control cell lines with unaltered expression of CD147, whereas HCC827-CD147-sh and H1975-CD147-sh cell lines with decreased expression of CD147 showed attenuated uptake of 18F-FDG compared to control counterparts. Data were from three independent tests. \bullet —CD147, \blacksquare —control, \blacklozenge —CD147-sh **(c)** Representative micro-PET/CT images of HCC827-CD147, HCC827-control, and HCC827-CD147-sh xenografts. Nude mice injected with lentiviral transduced HCC827 cell lines with different status of CD147 expression. 18F-FDG micro-PET/CT imaging was performed to determine the influence of CD147 on glucose uptake in vivo. The tumors were clearly visible, and more 18F-FDG accumulation was observed in HCC827-CD147 xenografts than in HCC827-control and HCC827-CD147-sh xenografts. **(d)** Histograms were drawn to identify the differences existed in SUVmax for xenografts developed from lentiviral transduced HCC827 cell lines with different status of CD147 expression. As shown, the SUVmax was dramatically higher in HCC827-CD147 xenografts than in HCC827-control and HCC827-CD147-sh xenografts. Compared to the HCC827-control xenografts, SUVmax was significantly decreased in the HCC827-CD147-sh xenografts. (***) $P < 0.001$.

Table 3 Correlation between CD147 and MCT1/4 expression in 70 LUAD tissues

Items		CD147 status			Total (n)	R	P-value
		±	++	+++			
MCT1 status	±	1	1	0	2	0.299	0.012
	++	4	19	17	40		
	+++	0	10	18	28		
Total (n)		5	30	35	70		
MCT4 status	±	2	4	1	7	0.463	<0.001
	++	3	20	14	37		
	+++	0	6	20	26		
Total (n)		5	30	35	70		

represents the most active metabolic location within the lesion, has been used as the most convenient metabolic parameter. Studies have shown that ^{18}F -FDG PET metabolic parameters are not only associated with survival and time to recurrence but also used as predictors for clinical

outcomes of lung cancer.^{26,27} Previous studies have shown that ^{18}F -FDG uptake was associated with genetic alterations in NSCLC, such as KRAS and EGFR mutation.^{28–30}

CD147 as a tumor-associated antigen is highly enriched on the surface of various malignant tumor cells, such as

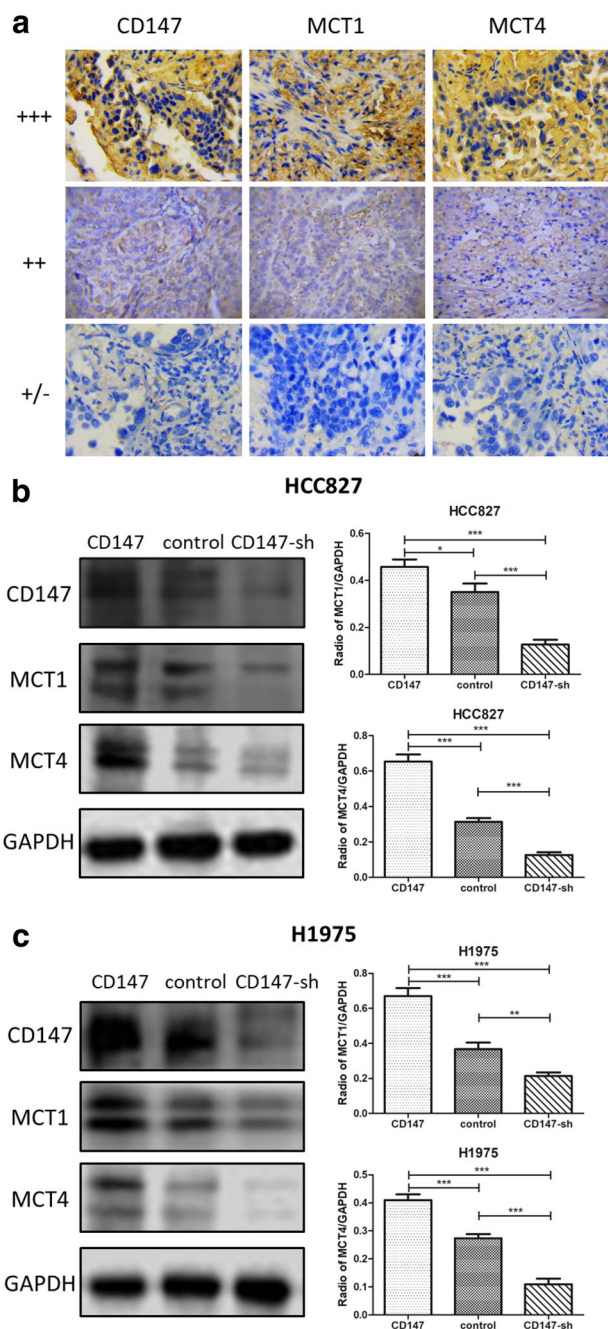


Figure 5 (a) Representative IHC images of CD147 and MCT1/4. (b) MCT1 and MCT4 expression levels were investigated in lentiviral transduced HCC827 cell lines by western blotting. The MCT1/GAPDH and MCT4/GAPDH ratios simply represent the level of MCT1 and MCT4 in stable HCC827 cell lines. Both ratios were considerably higher in established HCC827-CD147 cell lines than in HCC827-control and HCC827-CD147-sh cell lines. (c) Consistent with stable HCC827 cell lines, both MCT1/GAPDH and MCT4/GAPDH ratios were dramatically upregulated in the H1975-CD147 cell line. However, both ratios were extremely reduced in the H1975-CD147-sh cell line. (* $P < 0.05$, ** $P < 0.01$, *** $P < 0.001$).

lung cancer, ovarian cancer, liver cancer, breast cancer, and pancreatic cancer cells.³¹ Several lines of previous studies have shown that CD147 is a crucial regulator of glucose metabolism in hepatocellular carcinoma (HCC), thyroid cancer (TC), and NSCLC.¹⁷⁻¹⁹ According to Huang *et al.*,¹⁷ CD147 significantly contributes to the reprogramming of glucose metabolism in HCC cells through a p53-dependent pathway, which suggests the pivotal role of CD147 in the process of tumor-associated glycolysis. Huang *et al.* explored the molecular mechanisms that CD147 plays in TC, and their research indicated that miR-125a-5p regulates CD147, and through direct repression of the expression of the CD147 protein, miR-125a-5p suppresses aerobic glycolysis and lactate production and subsequently reduces TC cell viability, migration, and invasion, thereby exerting tumor suppressor functions.¹⁸ The results from a study by Li *et al.* provide in vitro and in vivo evidence that CD147-mediated glucose metabolic regulation via the Akt/mTOR-dependent pathway significantly correlates with EGFR-TKI treatment sensitivity prediction in NSCLC using ¹⁸F-FDG PET/CT imaging.¹⁹ Nevertheless, there is no definitive clinical evidence which supports that ¹⁸F-FDG PET/CT imaging is associated with CD147 in LUAD. In the present study, we detected CD147 expression via IHC staining in a group of 70 LUAD tissues and analyzed the relationship between CD147 expression and PET metabolic parameters. Our clinical observations that CD147 expression positively correlates with ¹⁸F-FDG PET metabolic parameters indicate that CD147 contributes to the reprogramming of glucose metabolism in LUAD. We therefore further conducted in vitro and in vivo experiments. Consistently, CD147 promoted ¹⁸F-FDG uptake by LUAD cell lines in vitro and the radioactive accumulation of ¹⁸F-FDG in LUAD xenografts in vivo, which revealed the importance of CD147 activity in glucose metabolism in LUAD.

Different anti-CD147 antibodies have been tested in tumors including HCC and head and neck squamous cancer (HNSC).³²⁻³⁴ He *et al.* reported that Licartin conjugated with I¹³¹ to the CD147 antibody can specifically recognize the CD147 antigen and significantly blocks cell invasion and growth in HCC cells.³² In 2016, a small molecule compound AC-73 was identified, and this compound binds to the N-terminal IgC2 domain of CD147 and prevents CD147 dimerization, which results in diminished motility and loss of invasiveness in HCC cells.³³ Furthermore, a chimeric CD147 antibody, named CNTO3899, dramatically inhibited HNSC cell proliferation and induced apoptosis in an ex vivo HNSC model.³⁴ In general, targeting CD147 is a novel strategy for antitumor therapy in HCC and HNSC. The results of the present study from clinical samples and cell lines indicate that CD147 promoted glucose

metabolism in LUAD and might be a candidate therapeutic target for LUAD. Clinically, early response prediction and short-term outcome prognosis of targeting therapy are essential to further individualizing therapy. Given the limitations in determining CD147 activity due to tissue availability and tumor heterogeneity, ¹⁸F-FDG PET/CT, as a reliable, simple, and noninvasive imaging modality, has the strength to detect early molecular responses to anti-CD147 antibodies. In addition, with the development of artificial intelligence and PET radiomics, many quantitative features from medical images, not just traditional metabolic parameters, can be extracted and analyzed to demonstrate the genetic alterations within tumor lesions and the efficacy of targeted drugs earlier.

As mentioned above, cancer cells undergo enhanced aerobic glycolysis, even in the presence of sufficient oxygen. The high glycolytic rate results in the production and accumulation of lactate within tumors. To avoid intracellular acidification and apoptosis, glycolytic cells must sustain lactate homeostasis.³⁵ MCTs play an important role through their involvement in lactic acid transportation.³⁶ In addition, cellular expression levels of MCT1 and MCT4 have been reported to correlate with the invasion activity of human lung cancer cells.³⁷ Although the regulation of MCT expression is still not fully understood, previous results have indicated that one of the best-characterized mechanisms of MCT regulation occurs through co-expression with CD147.³⁸ MCT1 and MCT4 directly bind to the transmembrane and cytoplasmic regions of CD147, which play a well-established role in trafficking MCTs to the plasma membrane for proper function. This interaction aids in the transportation of lactate across the plasma membrane and could play an important role in pH homeostasis in the tumor microenvironment. Given the close interaction between CD147 and MCT1 and MCT4 in cell metabolism regulation, we deduced that a clear functional role of CD147 in LUAD cells is its interaction with MCT1 and MCT4 involved in enhanced aerobic glycolysis. In our study, the IHC detection of CD147, MCT1, and MCT4 in clinical specimens showed a significant positive correlation. Consistently, western blot results also reveal that MCT expression was positively associated with CD147 in human LUAD cell lines.

Certainly, there were several limitations in this study. First, the clinical specimen was small-scale, since strict criteria were enacted to guarantee consistency in the basic condition of selected patients. Second, only the radioactive uptake of ¹⁸F-FDG by LUAD cell lines and corresponding xenografts was assessed to determine tumor glucose metabolic regulation. Third, the signal transduction pathway mechanisms responsible for the CD147-mediated enhancement of tumor glucose metabolism were not further investigated.

In conclusion, we investigated CD147-mediated glucose metabolic regulation in LUAD and its association with ¹⁸F-FDG PET/CT imaging. The results revealed that CD147 promoted glucose metabolism relying on MCT1 and MCT4, which suggests it might be a candidate target for LUAD therapy. Furthermore, with the increased importance of ¹⁸F-FDG PET/CT in supervising tumor response to anticancer drugs, ¹⁸F-FDG PET/CT is overwhelmingly superior in predicting and monitoring the therapeutic response to a novel antibody targeting CD147 with reasonable accuracy and reproducibility, which allows individualized therapy and, thus, more favorable therapeutic outcomes.

Acknowledgments

This work was supported by grants from the National Natural Science Foundation of China (2018ZX09201015, 81601377, 81501984), the Tianjin Natural Science Fund (16JCZDJC35200, 17JCYBJC25100, 18PTZWHZ00100, H2018206600), the Science & Technology Development Fund of Tianjin Education Commission for Higher Education (2018KJ057, 2018KJ061), the Tianjin Medical University Cancer Institute and Hospital Fund (Y1601, B1605, B1719, Y1805, Y1810) and the Incubation Project of the National Clinical Research Center for Cancer (N14B09).

Disclosure

The authors report there are no conflicts of interest.

References

- 1 Siegel RL, Miller KD, Jemal A. Cancer statistics, 2019. *CA Cancer J Clin* 2019; **69**: 7–34.
- 2 Gridelli C, Rossi A, Carbone DP *et al.* Non-small-cell lung cancer. *Nat Rev Dis Primers* 2015; **1**: 15009.
- 3 Hutchinson BD, Shroff GS, Truong MT, Ko JP. Spectrum of lung adenocarcinoma. *Semin Ultrasound CT MR* 2019; **40**: 255–64.
- 4 Dolly SO, Collins DC, Sundar R, Popat S, Yap TA. Advances in the development of molecularly targeted agents in non-small-cell lung cancer. *Drugs* 2017; **77**: 813–27.
- 5 Pavlova NN, Thompson CB. The emerging hallmarks of cancer metabolism. *Cell Metab* 2016; **23**: 27–47.
- 6 Vander Heiden MG, Cantley LC, Thompson CB. Understanding the Warburg effect: The metabolic requirements of cell proliferation. *Science* 2009; **324**: 1029–33.
- 7 Schwartz L, Supuran CT, Alfarouk KO. The Warburg effect and the hallmarks of cancer. *Anticancer Agents Med Chem* 2017; **17**: 164–70.

- 8 Plathow C, Weber WA. Tumor cell metabolism imaging. *J Nucl Med* 2008; **49**: 43S–63S.
- 9 Busk M, Horsman MR, Jakobsen S et al. Cellular uptake of PET tracers of glucose metabolism and hypoxia and their linkage. *Eur J Nucl Med Mol Imaging* 2008; **35**: 2294–303.
- 10 Biswas C, Zhang Y, DeCastro R et al. The human tumor cell-derived collagenase stimulatory factor (renamed EMMPRIN) is a member of the immunoglobulin superfamily. *Cancer Res* 1995; **55**: 434–9.
- 11 Weidle UH, Scheuer W, Eggle D, Klostermann S, Stockinger H. Cancer-related issues of CD147. *Cancer Genomics Proteomics* 2010; **7**: 157–69.
- 12 Yin H, Shao Y, Chen X. The effects of CD147 on the cell proliferation, apoptosis, invasion, and angiogenesis in glioma. *Neurol Sci* 2017; **38**: 129–36.
- 13 Toole BP. The CD147-HYALURONAN Axis in cancer. *Anat Rec* 2019; May 14 [Epub ahead of print]. <https://doi.org/10.1002/ar.24147>.
- 14 Xin X, Zeng X, Gu H et al. CD147/EMMPRIN overexpression and prognosis in cancer: A systematic review and meta-analysis. *Sci Rep* 2016; **6**: 32804.
- 15 Matsumoto T, Nagashio R, Ryuge S et al. Basigin expression as a prognostic indicator in stage I pulmonary adenocarcinoma. *Pathol Int* 2018; **68**: 232–40.
- 16 Lian C, Guo Y, Zhang J, Chen X, Peng C. Targeting CD147 is a novel strategy for antitumor therapy. *Curr Pharm des* 2017; **23**: 4410–21.
- 17 Huang Q, Li J, Xing J et al. CD147 promotes reprogramming of glucose metabolism and cell proliferation in HCC cells by inhibiting the p53-dependent signaling pathway. *J Hepatol* 2014; **61**: 859–66.
- 18 Huang P, Mao LF, Zhang ZP et al. Down-regulated miR-125a-5p promotes the reprogramming of glucose metabolism and cell malignancy by increasing levels of CD147 in thyroid cancer. *Thyroid* 2018; **28**: 613–23.
- 19 Li X, Fu Q, Zhu Y et al. CD147-mediated glucose metabolic regulation contributes to the predictive role of (18) F-FDG PET/CT imaging for EGFR-TKI treatment sensitivity in NSCLC. *Mol Carcinog* 2019; **58**: 247–57.
- 20 Granja S, Marchiq I, Le Floch R et al. Disruption of BASIGIN decreases lactic acid export and sensitizes non-small cell lung cancer to biguanides independently of the LKB1 status. *Oncotarget* 2015; **6**: 6708–21.
- 21 Su J, Gao T, Jiang M et al. CD147 silencing inhibits tumor growth by suppressing glucose transport in melanoma. *Oncotarget* 2016; **7**: 64778–84.
- 22 Chandrashekar DS, Basher B, Balasubramanya SAH et al. UALCAN: A portal for facilitating tumor subgroup gene expression and survival analyses. *Neoplasia* 2017; **19**: 649–58.
- 23 Györfy B, Surowiak P, Budczies J, Lánczky A et al. Online survival analysis software to assess the prognostic value of biomarkers using transcriptomic data in non-small-cell lung cancer. *PLOS One* 2013; **8**: e82241.
- 24 Gharibvand L, Shavlik D, Ghamsary M et al. The association between ambient fine particulate air pollution and lung cancer incidence: Results from the AHSMOG-2 study. *Environ Health Perspect* 2017; **125**: 378–84.
- 25 Li X, Wang D, Yu L. Prognostic and predictive values of metabolic parameters of (18)F-FDG PET/CT in patients with non-small cell lung cancer treated with chemotherapy. *Mol Imaging* 2019; **18**: 1536012119846025.
- 26 Kwon W, Howard BA, Herndon JE, Patz EF Jr. FDG uptake on positron emission tomography correlates with survival and time to recurrence in patients with stage I non-small-cell lung cancer. *J Thorac Oncol* 2015; **10**: 897–902.
- 27 Tönnies S, Tönnies M, Kollmeier J et al. Impact of preoperative 18F-FDG PET/CT on survival of resected mono-metastatic non-small cell lung cancer. *Lung Cancer* 2016; **93**: 28–34.
- 28 Caicedo C, Garcia-Veloso MJ, Lozano MD et al. Role of [¹⁸F]FDG PET in prediction of KRAS and EGFR mutation status in patients with advanced non-small-cell lung cancer. *Eur J Nucl Med Mol Imaging* 2014; **41**: 2058–65.
- 29 Kim YI, Paeng JC, Park YS et al. Relation of EGFR mutation status to metabolic activity in localized lung adenocarcinoma and its influence on the use of FDG PET/CT parameters in prognosis. *Am J Roentgenol* 2018; **210**: 1346–51.
- 30 Zhu L, Yin G, Chen W et al. Correlation between EGFR mutation status and F(18) -fluorodeoxyglucose positron emission tomography-computed tomography image features in lung adenocarcinoma. *Thorac Cancer* 2019; **10**: 659–64.
- 31 Riethdorf S, Reimers N, Assmann V et al. High incidence of EMMPRIN expression in human tumors. *Int J Cancer* 2006; **119**: 1800–10.
- 32 He Q, Lu WS, Liu Y, Guan YS, Kuang AR. 131I-labeled metuximab combined with chemoembolization for unresectable hepatocellular carcinoma. *World J Gastroenterol* 2013; **19**: 9104–10.
- 33 Fu ZG, Wang L, Cui HY et al. A novel small-molecule compound targeting CD147 inhibits the motility and invasion of hepatocellular carcinoma cells. *Oncotarget* 2016; **7**: 9429–47.
- 34 Dean NR, Knowles JA, Helman EE et al. Anti-EMMPRIN antibody treatment of head and neck squamous cell carcinoma in an ex-vivo model. *Anticancer Drugs* 2010; **21**: 861–7.
- 35 Kennedy KM, Dewhirst MW. Tumor metabolism of lactate: The influence and therapeutic potential for MCT and CD147 regulation. *Future Oncol* 2010; **6**: 127–48.
- 36 Pinheiro C, Longatto-Filho A, Azevedo-Silva J, Casal M, Schmitt FC, Baltazar F. Role of monocarboxylate transporters in human cancers: State of the art. *J Bioenerg Biomembr* 2012; **44**: 127–39.
- 37 Izumi H, Takahashi M, Uramoto H et al. Monocarboxylate transporters 1 and 4 are involved in the invasion activity of human lung cancer cells. *Cancer Sci* 2011; **102**: 1007–13.
- 38 Voss DM, Spina R, Carter DL, Lim KS, Jeffery CJ, Bar EE. Disruption of the monocarboxylate transporter-4-basigin interaction inhibits the hypoxic response, proliferation, and tumor progression. *Sci Rep* 2017; **7**: 4292.

Supporting Information

Additional Supporting Information may be found in the online version of this article at the publisher's website:

Table S1. Comparison of PET metabolic parameters between different expression groups of CD147. **Table S2.** Comparison of

PET metabolic parameters between different expression groups of MCT1/4. **Table S3.** Correlation between MCT1 expression and PET metabolic parameters in 70 LUAD tissues. **Table S4.** Correlation between MCT4 expression and PET metabolic parameters in 70 LUAD tissues.